

Geophysical Research Letters[®]













RESEARCH LETTER

10.1029/2022GL102633

Thomas J. Aubry and Samantha L. Engwell authors contributed equally to the publication and either of their names can be used first when citing this work.

New Insights Into the Relationship Between Mass Eruption Rate and Volcanic Column Height Based On the IVESPA Data Set

Thomas J. Aubry^{1,2} , Samantha L. Engwell³ , Costanza Bonadonna⁴ , Larry G. Mastin⁵ , Guillaume Carazzo⁶ , Alexa R. Van Eaton⁵ , David E. Jessop^{6,7} , Roy G. Grainger⁸, Simona Scollo⁹, Isabelle A. Taylor⁸ , A. Mark Jellinek¹⁰ , Anja Schmidt^{11,12,13}, Sébastien Biass⁴ , and Mathieu Gouhier⁷

Key Points:

- We provide empirical scaling relationships between mass eruption rate (MER) and column height using a new database with 134 volcanic events
- We constrain bespoke relationships and their uncertainties for four height metrics to support ash dispersion forecasters and researchers
- We detect no clear atmospheric influence on scaling relationships, highlighting required improvements of scaling models and the database

¹Now at Department of Earth and Environmental Sciences, University of Exeter, Penryn, UK, ²Sidney Sussex College, University of Cambridge, Cambridge, UK, ³British Geological Survey, The Lyell Centre, Edinburgh, UK, ⁴Department of Earth Sciences, University of Geneva, Geneva, Switzerland, ⁵Cascades Volcano Observatory, U.S. Geological Survey, Vancouver, WA, USA, ⁶Institut de Physique du Globe de Paris, Université Paris Cité, CNRS, Paris, France, ⁷OPGC Laboratoire Magmas et Volcans, Université Clermont Auvergne, CNRS, IRD, Clermont-Ferrand, France, ⁸COMET, Atmospheric, Oceanic and Planetary Physics, University of Oxford, Oxford, UK, ⁹Istituto Nazionale di Geofisica e Vulcanologia, Osservatorio Etneo, Catania, Italy, ¹⁰Earth Ocean and Atmospheric Sciences, University of British Columbia, Vancouver, BC, Canada, ¹¹Institute of Atmospheric Physics (IPA), German Aerospace Center (DLR), Oberpfaffenhofen, Germany, ¹²Meteorological Institute, Ludwig Maximilian University of Munich, Munich, Germany, ¹³Department of Chemistry, University of Cambridge, Cambridge, UK

Supporting Information:

Supporting Information may be found in the online version of this article.

Correspondence to:

T. J. Aubry and S. L. Engwell,
t.aubry@exeter.ac.uk;
sameng@bgs.ac.uk

Citation:

Aubry, T. J., Engwell, S. L., Bonadonna, C., Mastin, L. G., Carazzo, G., Van Eaton, A. R., et al. (2023). New insights into the relationship between mass eruption rate and volcanic column height based on the IVESPA data set. *Geophysical Research Letters*, 50, e2022GL102633. <https://doi.org/10.1029/2022GL102633>

Received 22 DEC 2022

Accepted 7 JUL 2023

Author Contributions:

Conceptualization: Thomas J. Aubry, Samantha L. Engwell

Data curation: Thomas J. Aubry, Samantha L. Engwell, Costanza Bonadonna, Larry G. Mastin, Guillaume Carazzo, Alexa R. Van Eaton, David E. Jessop, Roy G. Grainger, Simona Scollo, Isabelle A. Taylor, A. Mark Jellinek, Anja Schmidt, Sébastien Biass, Mathieu Gouhier

Abstract Rapid and simple estimation of the mass eruption rate (MER) from column height is essential for real-time volcanic hazard management and reconstruction of past explosive eruptions. Using 134 eruptive events from the new Independent Volcanic Eruption Source Parameter Archive (IVESPA, v1.0), we explore empirical MER-height relationships for four measures of column height: spreading level, sulfur dioxide height, and top height from direct observations and as reconstructed from deposits. These relationships show significant differences and highlight limitations of empirical models currently used in operational and research applications. The roles of atmospheric stratification, wind, and humidity remain challenging to detect across the wide range of eruptive conditions spanned in IVESPA, ultimately resulting in empirical relationships outperforming analytical models that account for atmospheric conditions. This finding highlights challenges in constraining the MER-height relation using heterogeneous observations and empirical models, which reinforces the need for improved eruption source parameter data sets and physics-based models.

Plain Language Summary Explosive volcanic eruptions expel gas and tephra in the form of a volcanic column (or plume) that rises into the atmosphere. Two important metrics characterizing these eruptions are the maximum rise height and the eruptive intensity, that is, the rate at which material is emitted from the eruptive vent. Understanding the relationship between these parameters is critical for reconstructing past volcanic events and managing hazards during volcanic crises. In this study, we use a new database of well-characterized eruptions to constrain simple relationships between column height and eruptive intensity. We distinguish four different measurements of column height: the maximum height reached by tephra from observations and from analysis of deposits, the height at which ash spreads in the atmosphere, and the height reached by volcanic sulfur gases. We show that each height category has a distinct relationship with the eruption intensity, enabling volcanologists and risk managers to use the relationship most appropriate to the measurements available to them. Despite the improved level of detail, our data set cannot resolve any systematic influence of atmospheric conditions such as wind and humidity on eruption column height, highlighting difficulties in measuring volcanic eruption characteristics and understanding their dynamics.

1. Introduction

Mass eruption rate (MER) and eruptive column (also known as volcanic plume) height are critical for forecasting volcanic ash transport and dispersion during an eruption, and in turn for real-time management of volcanic hazards (e.g., Beckett et al., 2020; Dioguardi et al., 2020; Mastin et al., 2022). MER and column height are also common metrics for eruption size (Carey & Sigurdsson, 1989; Croweller et al., 2012; Newhall & Self, 1982). Although column height can often be directly observed, MER is more challenging to constrain (Dürig et al., 2018; Pioli & Harris, 2019). Satellite, radar, cameras, or infrasound sensors have been used to directly estimate MER in near

© 2023. The Authors.

This is an open access article under the terms of the [Creative Commons Attribution License](https://creativecommons.org/licenses/by/4.0/), which permits use, distribution and reproduction in any medium, provided the original work is properly cited.

Formal analysis: Thomas J. Aubry, Samantha L. Engwell
Investigation: Thomas J. Aubry, Samantha L. Engwell, Costanza Bonadonna, Larry G. Mastin, Guillaume Carazzo, Alexa R. Van Eaton, David E. Jessop
Methodology: Thomas J. Aubry, Samantha L. Engwell
Project Administration: Thomas J. Aubry, Samantha L. Engwell
Visualization: Thomas J. Aubry, Samantha L. Engwell
Writing – original draft: Thomas J. Aubry, Samantha L. Engwell
Writing – review & editing: Thomas J. Aubry, Samantha L. Engwell, Costanza Bonadonna, Larry G. Mastin, Guillaume Carazzo, Alexa R. Van Eaton, David E. Jessop, Roy G. Grainger, Simona Scollo, Isabelle A. Taylor, A. Mark Jellinek, Anja Schmidt, Sébastien Biass, Mathieu Gouhier

real-time (e.g., Bear-Crozier et al., 2020; Freret-Lorgeril et al., 2021; Mereu et al., 2022, 2023), but these pioneering applications are either not operational or limited to a few of the world's best-monitored volcanoes (e.g., Etna volcano, Italy). Therefore, computationally inexpensive empirical scaling relationships and one-dimensional (1D) eruptive column models remain the most common tools to estimate MER based on observed height. The scaling models are particularly widely applied owing to their simplicity.

The canonical scaling model is an empirical power law relationship between MER and column height (Mastin et al., 2009; Morton et al., 1956; Sparks, 1986; Wilson et al., 1978). Development of these empirical relationships—and eruptive column models in general (1D, 3D)—is limited by data sets with a narrow range of eruptive and atmospheric parameters, absent or sparse information on uncertainty, and the use of dependent data, for example, when MER is derived from height. To address these issues, the Commission on Tephra Hazard Modeling of the International Association of Volcanology and Chemistry of the Earth's Interior (IAVCEI) developed the Independent Volcanic Eruption Source Parameter Archive (IVESPA, Aubry et al., 2021). Here, we use IVESPA to explore new empirical relationships between MER and the height of both tephra and SO₂ eruption columns and compare these results with analytical scaling models that account for atmospheric conditions.

2. Overview of IVESPA

We use version 1.0 of IVESPA (<http://www.ivespa.co.uk/>, Aubry et al., 2021). It contains 134 eruptive events, that is, eruption or eruption phases for which we have estimates of tephra fall deposit mass, duration, atmospheric conditions, and column height. Using the classification of Bonadonna and Costa (2013), 111 events are small-moderate, 18 are sub-Plinian and 5 are Plinian. IVESPA uses the following height metrics (see Figure 2 in Aubry et al., 2021):

- H_{top} , the height of the top of the tephra column, available for 130 events
- H_{spr} , the spreading height of the tephra cloud, available for 41 events
- H_{so_2} , the height of SO₂ injection, available for 28 events.

Height values provided in km above sea level (a.s.l.) in IVESPA have been converted to km above vent level (a.v.l.) for this study. The measurement techniques used to estimate column heights (e.g., ground based radar, satellite or visual observations) are reported although a single best estimate based on all available measurements is provided. Estimates of column heights, tephra mass, and duration are independent, for example, tephra mass was not estimated by inverting information from column height. We define the MER as the mass of tephra fallout (excluding pyroclastic density currents) derived from mapping the deposits and empirical fitting of the thinning trends (e.g., Bonadonna & Costa, 2012), divided by the eruptive event duration. MER is thus a time-averaged value, and we denote it $\overline{\text{MER}}$. For consistency, IVESPA provides observed column height from the published record that are also representative of a time-averaged value, denoted by $\overline{H}_{\text{top}}$, $\overline{H}_{\text{spr}}$ and $\overline{H}_{\text{so}_2}$. Most eruptive events do not have continuous time series of height, resulting in challenges in estimating the true time-averaged value (Aubry et al., 2021).

IVESPA parameters are assigned uncertainties representative of a 95% confidence level (Aubry et al., 2021). Both the best estimates and uncertainties are assigned an interpretation flag value between 0 (no interpretation) and 2 (heavy interpretation of the data source(s)). Events where parameters could not be estimated based on information in the literature were not included in the data set. Atmospheric profiles from two climate reanalyses are provided and are time-averaged over each event duration. IVESPA also contains vertically averaged (between the vent and $\overline{H}_{\text{top}}$) values of the horizontal wind speed (\overline{W}) and stratification (Brunt-Väisälä frequency, \overline{N}). The mean value from both atmospheric reanalyses is used as the best estimate, and their difference (halved) as the uncertainty. Table S1 contains all parameters used in this study and their calculation is detailed in Supporting Information S1 unless directly provided in IVESPA.

Top column heights are commonly estimated from deposits using isopleth contours (e.g., Carey & Sparks, 1986), which are excluded from IVESPA. However, for this study, we compile available top heights determined from isopleth maps for 18 eruptive events in IVESPA. We denote isopleth-derived heights $H_{\text{iso,top}}$ and do not bar the symbol because they are commonly representative of the maximum rather than time-averaged column height (e.g., Burden et al., 2011). For consistency, we use $H_{\text{iso,top}}$ estimated using the Carey and Sparks (1986) method rather than more recent and comprehensive methods (Rossi et al., 2019) that have been applied to a limited number of events. Text S2 in Supporting Information S1 and Table S2 provide detail on $H_{\text{iso,top}}$ data collection

using Alfano et al. (2011, 2016), Andronico et al. (2014), Bonadonna, Cioni, et al. (2015), Bourdier et al. (1997), Burden et al. (2011), Carey and Sigurdsson (1986), Carey et al. (1990), Castruccio et al. (2016), Eychenne et al. (2012), Kratzmann et al. (2010), Maeno et al. (2014, 2019), Naranjo et al. (1986), Romero et al. (2018), Rosi et al. (2001), and Self and Rampino (2012).

3. Methodology

New empirical power law models were defined between $\overline{H}_{\text{top}}$, $\overline{H}_{\text{spr}}$, $\overline{H}_{\text{SO}_2}$ and $H_{\text{iso,top}}$ and mass eruption rate $\overline{\text{MER}}$ in MATLAB™ using a non-linear least-squares fit procedure. We provide each model's: (a) confidence interval, reflecting the uncertainty on the fitted parameters and used to test if two models are significantly different; and (b) prediction intervals, reflecting the uncertainty on predictions based on both the uncertainty on the model parameters and the model error. All uncertainties and intervals are at the 95% confidence level. Information on all new empirical models is provided in Table S3.

Unlike empirical relationships, several analytical (derived from buoyant plume theory) scaling models explicitly account for atmospheric conditions (e.g., \overline{N} and \overline{W}). We use IVESPA to evaluate five of these models (Aubry et al., 2017; Degruyter & Bonadonna, 2012; Hewett et al., 1971; Morton et al., 1956; Woodhouse et al., 2013; see Table 1 and Text S3 in Supporting Information S1), as well as the empirical relationship from Mastin et al. (2009). We use the adjusted coefficient of determination (R_{adj}^2 , penalizing models with more independent variables) to compare model performance. Our key results (Table 1) are unchanged when using the bias-corrected Akaike Information Criterion instead (Table S4 in Supporting Information S1), which is generally more appropriate than R_{adj}^2 for non-linear models (Spiess & Neumeier, 2010). To account for eruption source parameter uncertainties and IVESPA biases, we repeated model evaluation with different set of weights applied to IVESPA events (Section 4.2, Table 1; weight expressions in Text S4 in Supporting Information S1):

- “Eruption” (column 4, Table 1): The same weight is given to each eruption in IVESPA reducing the influence of eruptions with numerous events (e.g., 18 events for the 1989–1990 Redoubt eruption)
- “Uncertainty” (column 5, Table 1): Weights are inversely proportional to the uncertainty on the observed and predicted $\overline{H}_{\text{top}}$ values for each event.
- “Interpretation Flag” (column 6, Table 1): Less weight is given to events that required heavy interpretation of the literature to attribute $\overline{H}_{\text{top}}$ and $\overline{\text{MER}}$ values.
- “All” (column 7, Table 1): The weight for each event is proportional to the product of the weights described above in columns 4–6 to account for all three factors.

4. Results

4.1. Empirical Scaling Relationships Specific to Different Column Height Metrics

Figures 1a–1d shows how $\overline{H}_{\text{top}}$ (a), $\overline{H}_{\text{spr}}$ (b), $\overline{H}_{\text{SO}_2}$ (c) and $H_{\text{iso,top}}$ (d) relate to $\overline{\text{MER}}$, and corresponding empirical power law relationships. $\overline{\text{MER}}$ values in IVESPA range from 2×10^1 – 2×10^8 kg s^{−1} (median: 1.6×10^6 kg s^{−1}), which is a larger range with a higher proportion of low-intensity events compared to previous studies (e.g., Mastin et al., 2009: $\overline{\text{MER}}$ range of 6×10^3 – 2×10^8 kg s^{−1} with median of 10^7 kg s^{−1}). Defining $\overline{\text{MER}}$ using the total mass of tephra (i.e., including pyroclastic density current contributions instead of fallout only) results in lower R^2 (Figure S1 in Supporting Information S1). For the $\overline{\text{MER}} - \overline{H}_{\text{top}}$ fit constrained by 130 events, we find best-fit relationships between the $\overline{\text{MER}}$ in kg s^{−1} and $\overline{H}_{\text{top}}$ in km above vent level (a.v.l.) of:

$$\overline{H}_{\text{top}} = 0.345 \times \overline{\text{MER}}^{0.226} \quad (1)$$

with the $\overline{\text{MER}}$ as independent variable, and

$$\log(\overline{\text{MER}}) = 2.83 + 3.54 \times \log(\overline{H}_{\text{top}}), \text{ equivalent to } \overline{H}_{\text{top}} = 0.159 \times \overline{\text{MER}}^{0.283} \quad (2)$$

with $\overline{H}_{\text{top}}$ as the independent variable and using a log-linear fit. Parameters in Equation 1 are most sensitive to events with high $\overline{\text{MER}}$ values (Figure S2 in Supporting Information S1). Best fits for all other types of height are provided in Figures 1e and 1f and Table S3, which aims to facilitate use of the new empirical fits, in particular by Volcanic Ash Advisory Centers (VAACs) and Volcano Observatories (VOs). Log-linear fits obtained using any

Table 1
 R^2_{adj} and Calibrated Parameter Values for Tested Scaling Models, for Various Weights Applied to Each Independent Volcanic Eruption Source Parameter Archive Event (See Section 2 and Text S4 in Supporting Information S1)

Reference	Expression for \bar{H}_{top}	Weighting procedure			
		Unweighted	Eruption	Uncertainty	Interpretation flag
Empirical power law with coefficients from Mastin et al. (2009)	$0.304 \overline{\text{MER}}^{0.241}$	$R^2_{\text{adj}} = 0.62$	$R^2_{\text{adj}} = 0.67$	$R^2_{\text{adj}} = 0.68$	$R^2_{\text{adj}} = 0.65$
Empirical power law with coefficients calibrated herein	a $\overline{\text{MER}}^b \bar{N}^c \bar{W}^d$	$R^2_{\text{adj}} = 0.67, a = 0.34, b = 0.23$	$R^2_{\text{adj}} = 0.7, a = 0.46, b = 0.21$	$R^2_{\text{adj}} = 0.74, a = 0.23, b = 0.25$	$R^2_{\text{adj}} = 0.69, a = 0.32, b = 0.23$
Empirical power law accounting for wind and stratification	a $\overline{\text{MER}}^b \bar{N}^c \bar{W}^d$	$R^2_{\text{adj}} = 0.75, a = 89, b = 0.17, c = 1.1, d = -0.049$	$R^2_{\text{adj}} = 0.79, a = 1.2e + 02, b = 0.16, c = 1.1, d = -0.0048$	$R^2_{\text{adj}} = 0.75, a = 2.4, b = 0.24, c = 0.48, d = -0.013$	$R^2_{\text{adj}} = 0.74, a = 49, b = 0.18, c = 0.94, d = -0.07$
Morton et al. (1956)*	a $\overline{\text{MER}}^{0.25} \bar{N}^{-0.75}$	$R^2_{\text{adj}} = 0.49, a = 0.0091$	$R^2_{\text{adj}} = 0.51, a = 0.0095$	$R^2_{\text{adj}} = 0.68, a = 0.0087$	$R^2_{\text{adj}} = 0.53, a = 0.0094$
Hewett et al. (1971)*	a $\overline{\text{MER}}^{0.33} \bar{N}^{-0.66} \bar{W}^{-0.33}$	$R^2_{\text{adj}} = 0.32, a = 0.0072$	$R^2_{\text{adj}} = 0.29, a = 0.0069$	$R^2_{\text{adj}} = 0.58, a = 0.0084$	$R^2_{\text{adj}} = 0.42, a = 0.0077$
Degruyter and Bonadonna (2012)*	a $\overline{\text{MER}}^{0.25} \bar{N}^{-0.75} f_{D12}(V^*, b)$	$R^2_{\text{adj}} = 0.48, a = 0.0092, b = 0.052$	$R^2_{\text{adj}} = 0.5, a = 0.0089, b = -0.2$	$R^2_{\text{adj}} = 0.68, a = 0.0091, b = 0.11$	$R^2_{\text{adj}} = 0.54, a = 0.01, b = 0.27$
Woodhouse et al. (2013)*	a $\overline{\text{MER}}^{0.25} \bar{N}^{-0.75} f_{W13}(W_s, \beta(\alpha))$	$R^2_{\text{adj}} = 0.52, a = 0.011, \beta(\alpha) = -6.8$	$R^2_{\text{adj}} = 0.53, a = 0.011, \beta(\alpha) = -5.7$	$R^2_{\text{adj}} = 0.69, a = 0.01, \beta(\alpha) = -5.5$	$R^2_{\text{adj}} = 0.58, a = 0.011, \beta(\alpha) = -7.1$
Aubry et al. (2017)*	a $\overline{\text{MER}}^{0.25} \bar{N}^{-0.75} f_{A17}(W^*, \beta(\alpha))$	$R^2_{\text{adj}} = 0.51, a = 0.0099, \beta(\alpha) = 2.5$	$R^2_{\text{adj}} = 0.51, a = 0.0093, \beta(\alpha) = -0.43$	$R^2_{\text{adj}} = 0.69, a = 0.0099, \beta(\alpha) = 3.5$	$R^2_{\text{adj}} = 0.58, a = 0.011, \beta(\alpha) = 4.4$

Note. * indicate analytical models. Physical parameters V^* , W_s , W^* and $\beta(\alpha)$ and functional expressions f_{D12} , f_{W13} and f_{A17} are provided in Text S3 in Supporting Information S1. Orange shading highlights models with calibrated parameter values deemed non-physical. For all other models, bold text highlights the one that has the highest R^2_{adj} value.

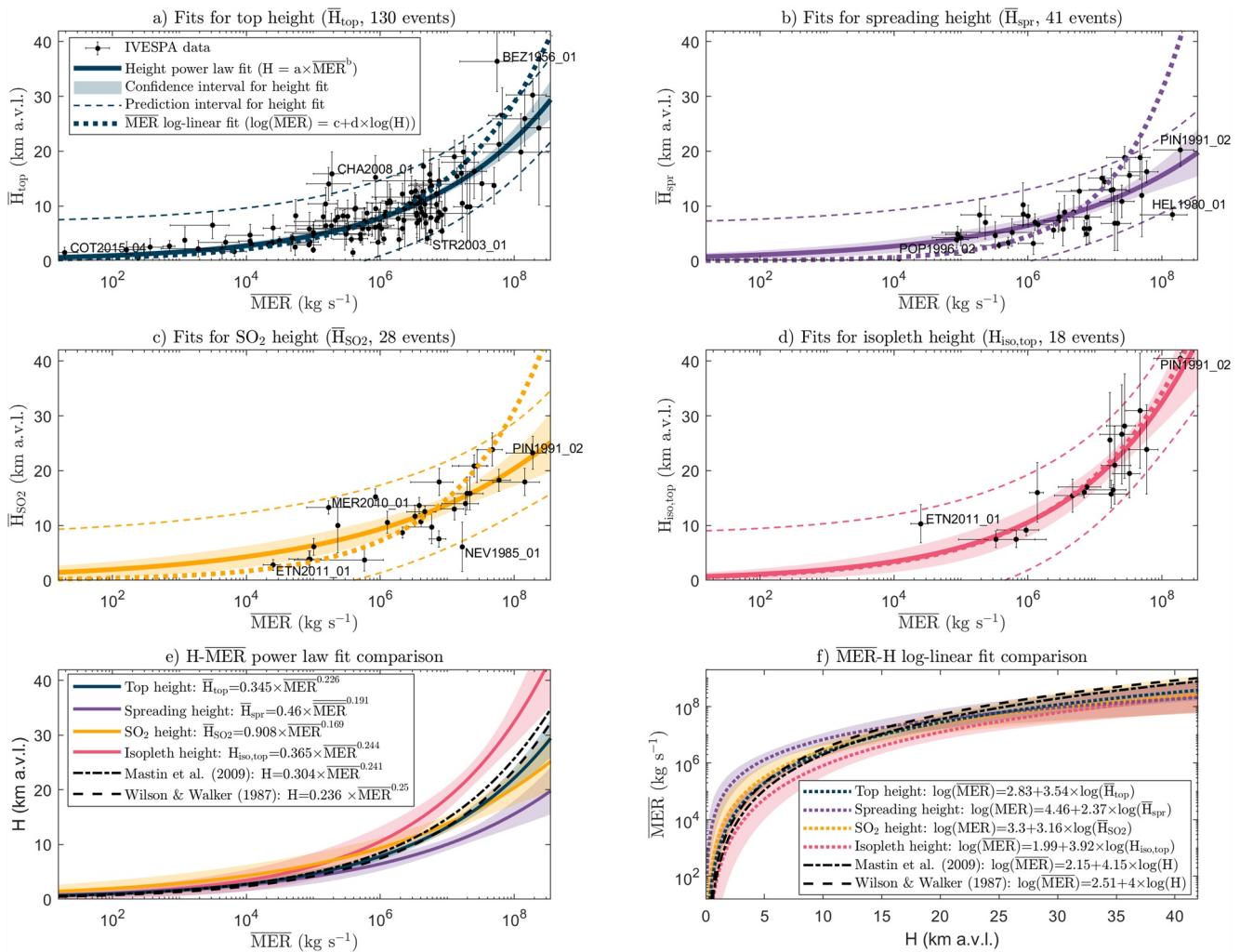


Figure 1. \bar{H}_{top} (a), \bar{H}_{spr} (b), \bar{H}_{SO_2} (c) and $H_{iso,top}$ (d) as a function of \bar{MER} . Panels (e) (power law fit, \bar{MER} as independent variable) and (f) (log linear fit, height as independent variable) compare the new empirical relationships for the four heights considered, along with relationships from Mastin et al. (2009) and Wilson and Walker (1987). Select events on panels (a)–(d) are labeled using their Independent Volcanic Eruption Source Parameter Archive (IVESPA) identifiers (see Table S1 for full details), for example, PIN1991_02 is phase 2 of the 1991 eruption of Mount Pinatubo.

of the considered heights as the independent variable generally predict significantly lower heights for low \bar{MER} and significantly higher heights for high \bar{MER} compared to equivalent power law fits calibrated with the \bar{MER} as the independent variable (Figures 1a–1d).

Figures 1e and 1f highlight important differences between empirical fits for different height metrics. For a given \bar{MER} value, the predicted $H_{iso,top}$ is significantly higher than the predicted \bar{H}_{top} (average $H_{iso,top}/\bar{H}_{top}$ ratio across IVESPA events = 1.45, Figure S3 in Supporting Information S1). This is consistent with the expectation that isopleth-based height reflects an upper bound of the top height, whereas IVESPA top column heights aim to reflect a time-averaged value. In addition, the method of Carey and Sparks (1986) tends to overestimate plume height for eruptions affected by strong wind (Rossi et al., 2019). Unsurprisingly, predicted \bar{H}_{spr} tends to be lower than predicted \bar{H}_{top} , with the average $\bar{H}_{spr}/\bar{H}_{top}$ ratio of 0.76 in IVESPA matching exactly that predicted by Morton et al. (1956) for buoyant plumes rising in quiescent environments (Figure S3 in Supporting Information S1). Predicted \bar{H}_{top} and \bar{H}_{SO_2} are generally not significantly different (average $\bar{H}_{\text{SO}_2}/\bar{H}_{top}$ ratio is 0.97 in IVESPA, Figure S3 in Supporting Information S1) and in the absence of other information, \bar{H}_{top} is an adequate metric for SO_2 injection height in gas dispersion and climate modeling studies.

The widely used empirical scaling of Mastin et al. (2009) compares best with our \bar{H}_{top} fit, although it is closer to our $H_{iso,top}$ fit at high \bar{MER} s for the power law fit (Figure 1e). This finding is unsurprising as although the plume

height type is unspecified in Mastin et al. (2009), most heights in the literature reflect top height values, and Mastin et al. (2009) included isopleth-based heights in their compilation (unlike IVESPA). There are statistically significant differences between Mastin et al. (2009) and our new top height fits (up to 15% for predicted $\overline{H}_{\text{top}}$ and up to 0.6 for predicted $\log(\overline{\text{MER}})$, that is, a factor of 4 for $\overline{\text{MER}}$). The relative root mean squared error (RMSE) on $\overline{H}_{\text{top}}$ (predicted from $\overline{\text{MER}}$) is 53% for Equation 1, 57% for Equation 2 and 60% for Mastin et al. (2009) (Figure S4a in Supporting Information S1). When using these relationships and observed $\overline{H}_{\text{top}}$ to invert for $\overline{\text{MER}}$, duration or tephra fallout mass (Figures S4b–S4d in Supporting Information S1), the RMSE on the predicted $\log(\overline{\text{MER}})$ is 0.81 for Equation 1, 0.76 for Equation 2 and 0.80 for Mastin et al. (2009). The new empirical relationships for $\overline{H}_{\text{top}}$ (Equations 1 and 2) are thus broadly consistent with Mastin et al. (2009). However, we show that the optimal parameter values of empirical scaling relationships and corresponding predictions differ greatly depending on the height metric (i.e., $\overline{H}_{\text{top}}$, $\overline{H}_{\text{spr}}$, $\overline{H}_{\text{SO}_2}$ or $H_{\text{iso,top}}$).

4.2. Accounting for Atmospheric Conditions Using Analytical Scaling Models

Table 1 (column 3) shows that the empirical power law outperforms analytical scaling models accounting for atmospheric conditions when giving the same weight to all events in IVESPA. The only model that outperforms the empirical relationship between $\overline{H}_{\text{top}}$ and $\overline{\text{MER}}$ (Equation 1, $R_{\text{adj}}^2 = 0.67$) is another empirical power law between $\overline{H}_{\text{top}}$, $\overline{\text{MER}}$, \overline{N} , and \overline{W} ($R_{\text{adj}}^2 = 0.75$). However, the obtained exponent for \overline{N} is 1.1, meaning that higher heights are predicted for stronger stratification values, which is an unphysical result (Morton et al., 1956). The analytical scaling models have R_{adj}^2 values between 0.32 and 0.52, much smaller than the empirical power law. This result is not explained by the use of the full IVESPA data set to both calibrate and test models (including the empirical power-law). If we split IVESPA into distinct calibration and evaluation data sets, we find a 99.6% probability that the R_{adj}^2 of the empirical power law exceeds that of any analytical scalings (Table S5 in Supporting Information S1).

The poor performance of analytical scaling relationships could be explained by poorly constrained parameter values in IVESPA, or the fact that multiple events from one eruption dominate the database. We find that weighting the data (Table 1, column 4–7) to account for these factors does not change the main results: (a) the empirical power law fit between $\overline{H}_{\text{top}}$ and $\overline{\text{MER}}$ outperforms (higher R_{adj}^2) the analytical models; and (b) the best-performing model is the empirical power law that includes \overline{N} and \overline{W} terms, with a positive (unphysical) exponent for \overline{N} . When weighting the eruptive events by parameter uncertainty, the performance of all scaling models improves, with greater improvement among the analytical models accounting for atmospheric conditions. For example, the difference in R_{adj}^2 values between the power-law fit and the best analytical scaling (Degruyter & Bonadonna, 2012) when applying all weighting procedures is 0.06, whereas it is 0.19 unweighted. For the power law fit, the $\overline{\text{MER}}$ exponent varies between 0.21 and 0.25 depending on the weighting procedures applied and is thus robust. However, fit parameters of analytical models are very sensitive to the weighting. For example, the calibrated value of entrainment coefficient ratio β/α in the Aubry et al. (2017) scaling model ranges between -0.43 (an unphysical value) and 4.4. Laboratory studies suggest that the ratio of β/α should be 0.6–20 (Aubry & Jellinek, 2018, and references therein).

5. Discussion

5.1. Influence of Atmospheric Conditions

Using 25 eruptive events, Mastin (2014) demonstrated that a 1D plume model accounting for atmospheric conditions was not as good as an empirical power-law in predicting $\overline{\text{MER}}$ from column height. Despite having improved data compilation methodologies and over five times more events in IVESPA, we reach similar conclusions as the simple $\overline{\text{MER}}-\overline{H}_{\text{top}}$ empirical power law outperforms analytical scaling models accounting for atmospheric conditions (Table 1). To understand this result, we define the standardized top height as $\overline{H}_{\text{top}}^{\text{std}} = \overline{H}_{\text{top}}/[0.0345 \overline{\text{MER}}^{0.226}]$, the ratio of observed $\overline{H}_{\text{top}}$ and the value predicted from $\overline{\text{MER}}$ using Equation 1. Figure 2a suggests that $\overline{H}_{\text{top}}^{\text{std}}$ does not depend on \overline{N} in IVESPA, whereas Table 1 even suggests that $\overline{H}_{\text{top}}$ increases with \overline{N} . These results contradict theoretical and experimental evidence that $\overline{H}_{\text{top}}$ should decrease in a more strongly stratified atmosphere (e.g., Morton et al., 1956; Woods, 1988), and cause the poor performance of analytical models in which $\overline{H}_{\text{top}}$ is proportional to $\overline{N}^{-0.75}$. One potential explanation is that \overline{N} generally increases with altitude (Figure

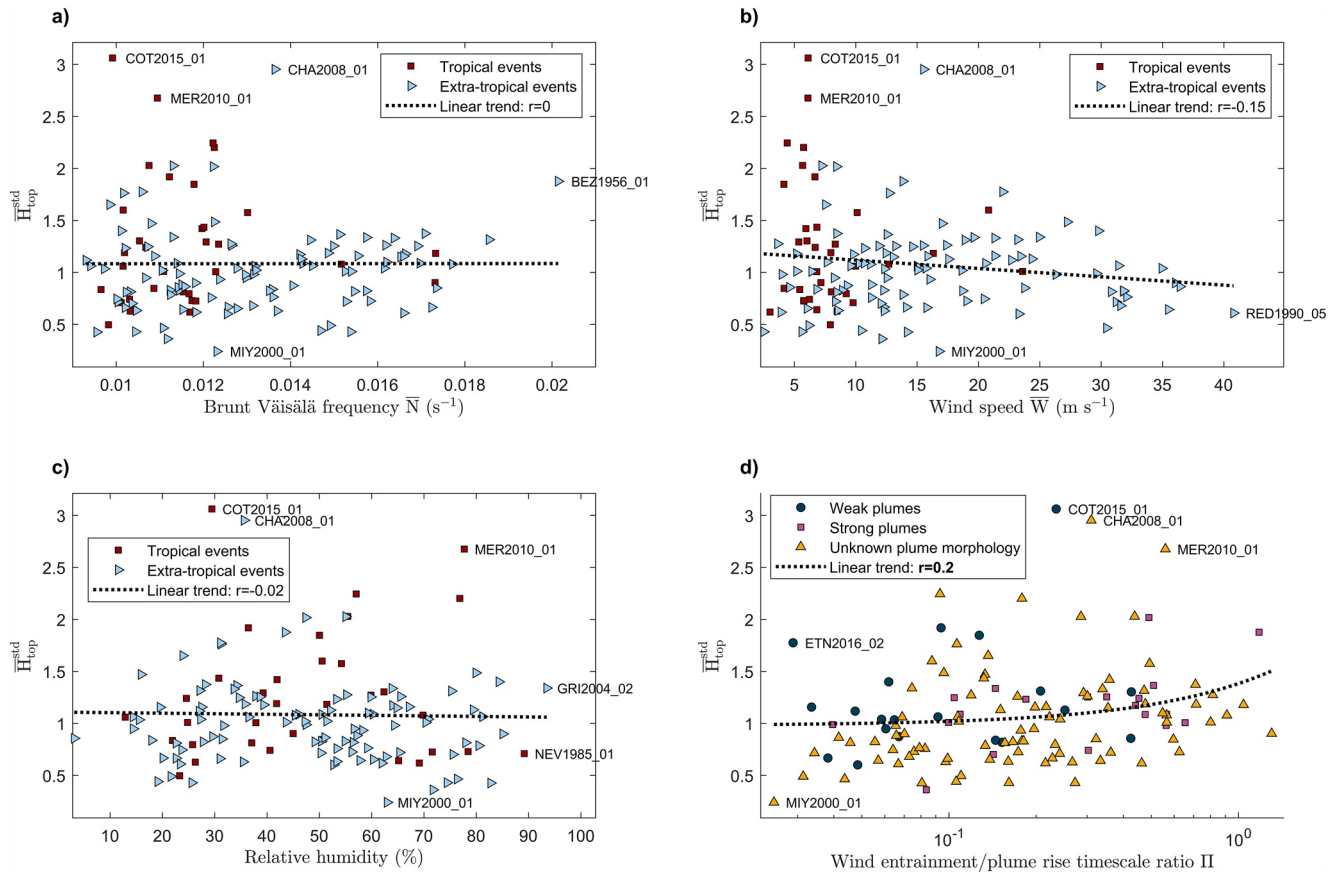


Figure 2. \overline{H}_{top}^{std} as a function of \overline{N} (a), \overline{W} (b), average relative humidity (c), and Π (d). (c) Linear correlation coefficient r is annotated on each panel (bold if significant at the 95% confidence level). The Independent Volcanic Eruption Source Parameter Archive identifier of select outsider events is annotated (Table 1).

S5a in Supporting Information S1) and in turn with \overline{H}_{top} and \overline{MER} . If \overline{N} is normalized for each event by the value obtained from the average atmospheric profile across IVESPA (which removes the dependence of \overline{N} on vent and column altitude), it becomes negatively although insignificantly correlated with \overline{H}_{top}^{std} (Figure S6a in Supporting Information S1).

Figure 2b shows that \overline{H}_{top}^{std} decreases with stronger horizontal wind speed \overline{W} , as expected from laboratory experiments (e.g., Carazzo et al., 2014; Hewett et al., 1971) and a few well-observed eruptions (e.g., Dürig et al., 2022; Poulidis et al., 2019), but that the two variables are not significantly correlated. We also do not detect any influence of relative humidity (Figure 3c), despite model predictions that the atmospheric water vapor entrained into a volcanic plume and the associated latent heat flux should boost \overline{H}_{top} by over 5 km for small-moderate eruptions in a wet tropical atmosphere (e.g., Glaze et al., 1997; Herzog et al., 1998; Tupper et al., 2009; Woods, 1993). Although several studies have noted that tropical volcanic plumes commonly reach the tropopause (e.g., Carboni et al., 2016; Tupper & Wunderman, 2009), without any constraint on MER as in this study, the role of humidity can only be speculated. Removing the influence of altitude on \overline{W} and relative humidity (Figure S5 in Supporting Information S1) only marginally increases their apparent influence on \overline{H}_{top}^{std} (Figure S6 in Supporting Information S1).

Last, we tested the influence of volcanic plume morphology (i.e., weak, bent-over and spreading downwind only, vs. strong, spreading both upwind and downwind). This parameter is constrained using direct observations (e.g., pictures, infrared cameras) for only 44 events in IVESPA, so we complement it by calculating

$$\Pi = \left(\frac{\alpha}{\beta}\right)^2 \frac{\overline{H}_{top} \overline{N}}{1.8 \overline{W}} \quad (3)$$

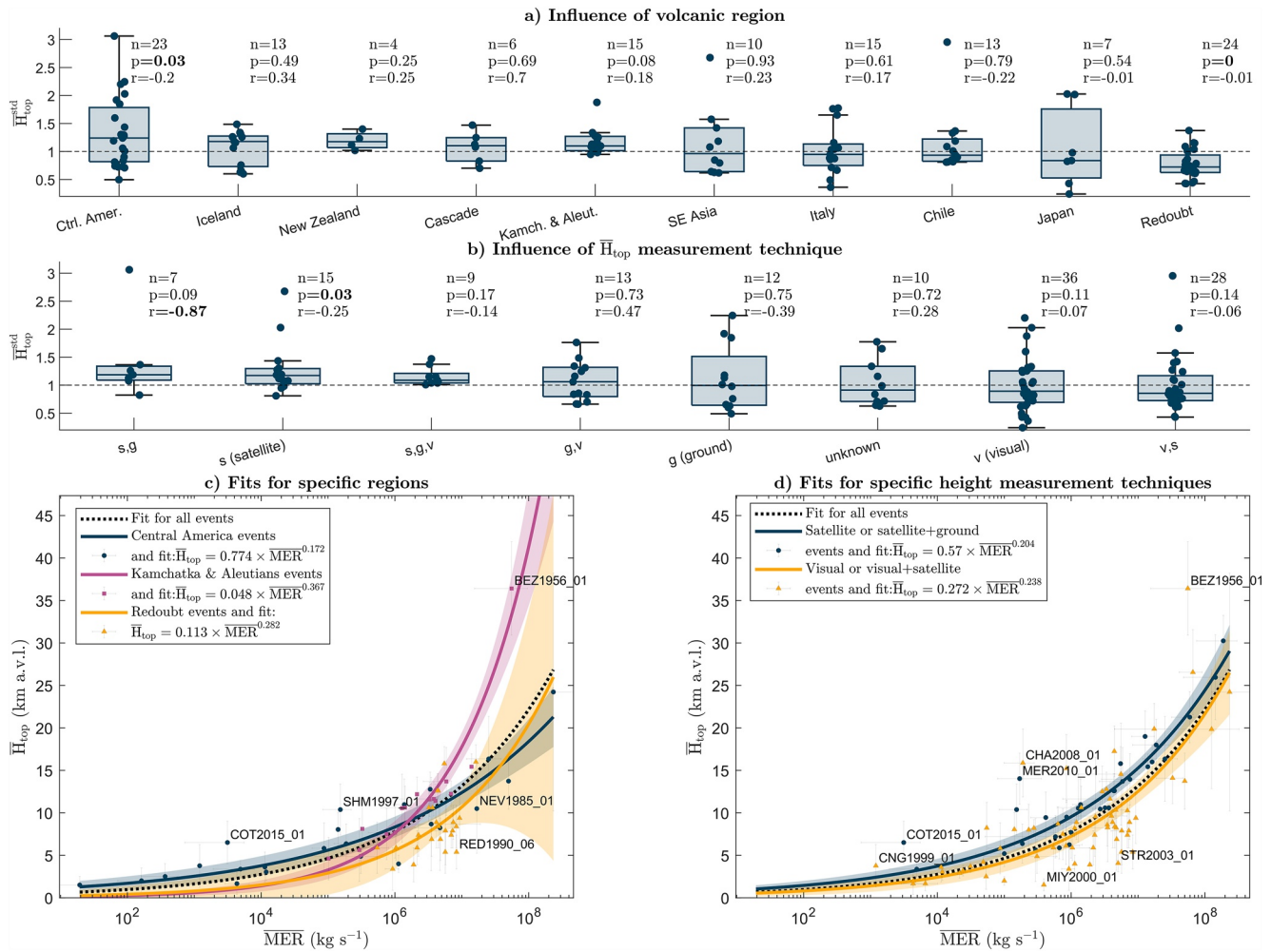


Figure 3. Distribution of \overline{H}_{top}^{std} for specific volcanic regions (a) or \overline{H}_{top} measurement techniques (b). Box plots show the minimum, quartiles, and maximum values. Three values are annotated for each subgroup: the number of events (n), the p -value resulting from a Mann-Whitney U-test testing the probability that values from the subgroup differ significantly from the values from all other subgroups (p), and the correlation coefficient between $\log(\overline{H}_{top}^{std})$ and $\log(\overline{W})$ (r) (r and p in bold if significant at the 95% level). Panels (c)–(d) are similar to Figure 1a, but show \overline{H}_{top} – \overline{MER} power law fits calibrated for select subgroups of regions (c) or measurement techniques (d).

for each event. Π is a non-dimensional parameter defined by the ratio of the wind entrainment and plume rise timescales (Degruyter & Bonadonna, 2012) and has been shown to relate to the plume morphology for a handful of eruptions (e.g., Bonadonna, Pistolesi, et al., 2015; Dürig et al., 2023; Scollo et al., 2019). We use $\alpha = 0.1$ and $\beta = 0.5$ in Equation 3, consistent with latest entrainment coefficient estimates (e.g., Aubry & Jellinek, 2018; Michaud-Dubuy et al., 2020). Values of Π in IVESPA range from 0.02 to 1.1 with weak plumes associated with lower values. Both types of plumes are found for $0.03 < \Pi < 0.35$ (Figure 2d and Figure S3 in Supporting Information S1), suggesting a transition from weak to strong plumes at a critical value of $\Pi \approx 0.1$. This value is considerably lower than that originally proposed in Bonadonna, Pistolesi, et al. (2015) for the 2011 Cordon Caulle eruption, Chile ($\Pi \approx 10$) but is in agreement with $\Pi = 0.5$ as found in recent studies for Etna (Scollo et al., 2019) and Eyjafjallajökull (Dürig et al., 2023). Despite the absence of any clear relationship between \overline{H}_{top}^{std} and Π in Figure 2d, the statistically significant correlation hints to a small but discernible influence of the plume morphology on the \overline{H}_{top} – \overline{MER} relationship.

5.2. Influence of Location and Column Height Measurement Technique

Figure 3a shows the distribution of \overline{H}_{top}^{std} for 10 geographical regions. Across these regions, the median \overline{H}_{top}^{std} varies between 0.72 and 1.24, that is, the median observed \overline{H}_{top} differs from the median value predicted using

Equation 1 by -28% (Redoubt) to $+24\%$ (Central America). The distributions of $\overline{H}_{\text{top}}^{\text{std}}$ for these two regions significantly differ compared to all other regions. Regional differences might reflect a range of factors including atmospheric conditions, the prevalence of certain magma or edifice types, or the prevalence of island volcanoes with limited deposition on land and low bias on the tephra fallout mass and $\overline{\text{MER}}$. Even when subdivided into 10 geographical areas, most still contain 10–24 events. We can thus calibrate region or volcano-specific $\overline{H}_{\text{top}}-\overline{\text{MER}}$ relationships and show select examples in Figure 3c.

Figure 3b shows the distribution of $\overline{H}_{\text{top}}^{\text{std}}$ for eight different combinations of measurement technique used to measure $\overline{H}_{\text{top}}$. $\overline{H}_{\text{top}}^{\text{std}}$ estimated from satellite-only measurements or a combination of satellite and ground-based instrumental measurements (e.g., radar) tend to be higher than for other measurement techniques (p -value < 0.1), consistent with Tupper and Wunderman (2009). In contrast, when visual measurements were used alone or in combination with satellite imagery, $\overline{H}_{\text{top}}^{\text{std}}$ tends to be lower (p -value < 0.15). Figure 3d shows that bespoke $\overline{H}_{\text{top}}-\overline{\text{MER}}$ relationships for these two categories (satellite vs. visual) differ at most $\overline{\text{MER}}$ values. The dependence of $\overline{H}_{\text{top}}^{\text{std}}$ on other parameters was explored with examples for duration, median grain size and tropopause height shown in Figures S7 and S8 in Supporting Information S1. The 17 events with a duration smaller than 10 times the plume rise timescale tend to have smaller $\overline{H}_{\text{top}}^{\text{std}}$ (Figure S7a in Supporting Information S1) but giving these short-duration events less weights does not change Table 1 results (not shown).

Last, among all sub-categories shown in Figure 3, the correlation coefficient between $\log(\overline{H}_{\text{top}}^{\text{std}})$ and $\log(\overline{W})$ is only significant for the subgroup of satellite and ground-based $\overline{H}_{\text{top}}$ measurement ($r = -0.87$). This emphasizes the difficulty of detecting atmospheric influence on the $\overline{H}_{\text{top}}-\overline{\text{MER}}$ relationship in IVESPA v1.0.

5.3. Future Eruption Data Requirements and IVESPA Developments

The challenging detection of atmospheric influence on the MER-height relationship in IVESPA v1.0 may be due to the use of simple scaling (0D) models, and future studies could investigate application of more sophisticated eruptive column models (1D, 3D) or data analysis techniques (e.g., machine learning) to IVESPA. However, our study hints at developments of IVESPA, and eruptive data more generally, that will help build a better understanding of the relationship between MER, column height and atmospheric conditions. First, Figure 3b shows that future versions of IVESPA should explicitly separate column heights according to measurement type. Second, Figure 3a and other studies suggest that compiling information such as magma composition or type (e.g., Trancoso et al., 2022) and conduit information (e.g., Gouhier et al., 2019) would help constrain other factors modulating the relationship between height and MER. Whether interpolation of large-scale reanalysis data sets to infer local atmospheric profile is adequate for plume modeling could be further tested. Last, the use of time-averaged eruption source parameters might prevent the detection of atmospheric influence on plume dynamics in a database with such a variety of eruptions. Advances in near real-time measurements of MER (Bear-Crozier et al., 2020; Caudron et al., 2015; Freret-Lorgeril et al., 2018, 2021; Mereu et al., 2022, 2023) are critical to build time-dependencies in global databases like IVESPA. These database development should aid understanding of the dynamics of volcanic plumes, and in particular detect and model the influence of atmospheric conditions (Section 5.1).

6. Conclusions

We used the new Independent Volcanic Eruption Source Parameter Archive (IVESPA, Aubry et al., 2021) to explore the empirical power law relationship linking column height to MER. A key improvement over previous work is that our new relationships are specific to the type of column height considered, that is, the height of the SO_2 cloud ($\overline{H}_{\text{SO}_2}$), the spreading height of the tephra cloud ($\overline{H}_{\text{spr}}$), and the top height of the ash cloud directly measured ($\overline{H}_{\text{top}}$) or derived from the distribution of the largest clasts ($H_{\text{iso,top}}$) with significant differences among these four metrics (Figure 1 and Figure S3 in Supporting Information S1). We provide a summary of all newly constrained empirical relationships, their uncertainties and look-up tables to facilitate application by a wide range of users including VAACs or VOs (Table S3). The newly calibrated power law relationship between $\overline{H}_{\text{top}}$ and $\overline{\text{MER}}$ (Equation 1) still results in discrepancies of 50% for predicted $\overline{H}_{\text{top}}$, and a factor of ~ 6 for predicted $\overline{\text{MER}}$. However, it still outperforms analytical scaling models accounting for atmospheric wind and stratification. It is important to note that empirical relationships will always provide information within the range of eruptions

considered and will evolve depending on the data set considered, while analytical models are designed to be of wider application. Discrepancies in the analytical scaling shown in our analysis might be related to both uncertainty in the data and uncertainty in the existing models. More work is required to better interpret these results and provide more accurate models. Further improvements to IVESPA might be needed to detect atmospheric influences on plume dynamics, but we may simply be identifying an inherent limitation in the accuracy with which secondary controls on plume dynamics can be captured in global databases using time-averaged plume heights or erupted mass by deposit mapping.

Data Availability Statement

All data and MATLAB™ scripts used in this study is available from a publicly available repository at <https://doi.org/10.5281/zenodo.8085934>, with scripts also available from GitHub at https://github.com/thomasaubry/IVESPA_GRL2023_scripts. The core data used is from the Independent Volcanic Eruption Source Parameter Archive (IVESPA) Version 1.0 at <http://ivespa.co.uk/data.html>. IVESPA is curated by the IAVCEI Commission on Tephra Hazard Modeling and supported by the British Geological Survey.

References

- Alfano, F., Bonadonna, C., Volentik, A. C., Connor, C. B., Watt, S. F., Pyle, D. M., & Connor, L. J. (2011). Tephra stratigraphy and eruptive volume of the May, 2008, Chaitén eruption, Chile. *Bulletin of Volcanology*, 73(5), 613–630. <https://doi.org/10.1007/s00445-010-0428-x>
- Alfano, F., Bonadonna, C., Watt, S., Connor, C., Volentik, A., & Pyle, D. M. (2016). Reconstruction of total grain size distribution of the climactic phase of a long-lasting eruption: The example of the 2008–2013 Chaitén eruption. *Bulletin of Volcanology*, 78(7), 1–21. <https://doi.org/10.1007/s00445-016-1040-5>
- Andronico, D., Scollo, S., Cristaldi, A., & Castro, M. D. L. (2014). Representativity of incompletely sampled fall deposits in estimating eruption source parameters: A test using the 12–13 January 2011 lava fountain deposit from Mt. Etna volcano, Italy. *Bulletin of Volcanology*, 76(10), 861. <https://doi.org/10.1007/s00445-014-0861-3>
- Aubry, T. J., Engwell, S., Bonadonna, C., Carazzo, G., Scollo, S., Van Eaton, A. R., et al. (2021). The Independent Volcanic Eruption Source Parameter Archive (IVESPA, version 1.0): A new observational database to support explosive eruptive column model validation and development. *Journal of Volcanology and Geothermal Research*, 417, 107295. <https://doi.org/10.1016/j.jvolgeores.2021.107295>
- Aubry, T. J., & Jellinek, A. M. (2018). New insights on entrainment and condensation in volcanic plumes: Constraints from independent observations of explosive eruptions and implications for assessing their impacts. *Earth and Planetary Science Letters*, 490, 132–142. <https://doi.org/10.1016/j.epsl.2018.03.028>
- Aubry, T. J., Jellinek, A. M., Carazzo, G., Gallo, R., Hatcher, K., & Dunning, J. (2017). A new analytical scaling for turbulent wind-bent plumes: Comparison of scaling laws with analog experiments and a new database of eruptive conditions for predicting the height of volcanic plumes. *Journal of Volcanology and Geothermal Research*, 343, 233–251. <https://doi.org/10.1016/j.jvolgeores.2017.07.006>
- Bear-Crozier, A., Pouget, S., Bursik, M., Jansons, E., Denman, J., Tupper, A., & Rustowicz, R. (2020). Automated detection and measurement of volcanic cloud growth: Towards a robust estimate of mass flux, mass loading and eruption duration. *Natural Hazards*, 101, 1–38. <https://doi.org/10.1007/s11069-019-03847-2>
- Beckett, F. M., Witham, C. S., Leadbetter, S. J., Crocker, R., Webster, H. N., Hort, M. C., et al. (2020). Atmospheric dispersion modelling at the London VAAC: A review of developments since the 2010 Eyjafjallajökull volcano ash cloud. *Atmosphere*, 11(4), 352. <https://doi.org/10.3390/atmos11040352>
- Bonadonna, C., Cioni, R., Pistolesi, M., Elissondo, M., & Baumann, V. (2015). Sedimentation of long-lasting wind-affected volcanic plumes: The example of the 2011 rhyolitic Cordón Caulle eruption, Chile. *Bulletin of Volcanology*, 77(2), 13. <https://doi.org/10.1007/s00445-015-0900-8>
- Bonadonna, C., & Costa, A. (2012). Estimating the volume of tephra deposits: A new simple strategy. *Geology*, 40(5), 415–418. <https://doi.org/10.1130/G32769.1>
- Bonadonna, C., & Costa, A. (2013). Plume height, volume, and classification of explosive volcanic eruptions based on the Weibull function. *Bulletin of Volcanology*, 75(8), 742. <https://doi.org/10.1007/s00445-013-0742-1>
- Bonadonna, C., Pistolesi, M., Cioni, R., Degruyter, W., Elissondo, M., & Baumann, V. (2015). Dynamics of wind-affected volcanic plumes: The example of the 2011 Cordón Caulle eruption, Chile. *Journal of Geophysical Research: Solid Earth*, 120(4), 2242–2261. <https://doi.org/10.1002/2014jb011478>
- Bourdier, J.-L., Prato, I., Thouret, J.-C., Boudon, G., & Vincent, P. M. (1997). Observations, stratigraphy and eruptive processes of the 1990 eruption of Kelut volcano, Indonesia. *Journal of Volcanology and Geothermal Research*, 79(3), 181–203. [https://doi.org/10.1016/S0377-0273\(97\)00031-0](https://doi.org/10.1016/S0377-0273(97)00031-0)
- Burden, R. E., Phillips, J. C., & Hincks, T. K. (2011). Estimating volcanic plume heights from depositional clast size. *Journal of Geophysical Research*, 116(B11), B11206. <https://doi.org/10.1029/2011JB008548>
- Carazzo, G., Girault, F., Aubry, T., Bouquerel, H., & Kaminski, E. (2014). Laboratory experiments of forced plumes in a density-stratified crossflow and implications for volcanic plumes. *Geophysical Research Letters*, 41(24), 8759–8766. <https://doi.org/10.1002/2014gl061887>
- Carboni, E., Grainger, R. G., Mather, T. A., Pyle, D. M., Thomas, G. E., Siddans, R., et al. (2016). The vertical distribution of volcanic SO₂ plumes measured by IASI. *Atmospheric Chemistry and Physics*, 16(7), 4343–4367. <https://doi.org/10.5194/acpd-15-24643-2015>
- Carey, S., & Sigurdsson, H. (1986). The 1982 eruptions of El Chichón volcano, Mexico (2): Observations and numerical modelling of tephra-fall distribution. *Bulletin of Volcanology*, 48(2–3), 127–141. <https://doi.org/10.1007/BF01046547>
- Carey, S., & Sigurdsson, H. (1989). The intensity of Plinian eruptions. *Bulletin of Volcanology*, 51(1), 28–40. <https://doi.org/10.1007/BF01086759>
- Carey, S., Sigurdsson, H., Gardner, J. E., & Criswell, W. (1990). Variations in column height and magma discharge during the May 18, 1980 eruption of Mount St. Helens. *Journal of Volcanology and Geothermal Research*, 43(1–4), 99–112. [https://doi.org/10.1016/0377-0273\(90\)90047-J](https://doi.org/10.1016/0377-0273(90)90047-J)
- Carey, S., & Sparks, R. S. J. (1986). Quantitative models of the fallout and dispersal of tephra from volcanic eruption columns. *Bulletin of Volcanology*, 48(2–3), 109–125. <https://doi.org/10.1007/BF01046546>

- Castruccio, A., Clavero, J., Segura, A., Samaniego, P., Roche, O., Le Pennec, J. L., & Drogue, B. (2016). Eruptive parameters and dynamics of the April 2015 sub-Plinian eruptions of Calbuco volcano (southern Chile). *Bulletin of Volcanology*, 78(9), 62. <https://doi.org/10.1007/s00445-016-1058-8>
- Caudron, C., Taisne, B., Garcés, M., Alexis, L. P., & Mialle, P. (2015). On the use of remote infrasound and seismic stations to constrain the eruptive sequence and intensity for the 2014 Kelud eruption. *Geophysical Research Letters*, 42(16), 6614–6621. <https://doi.org/10.1002/2015gl064885>
- Crowther, H. S., Arora, B., Brown, S. K., Cottrell, E., Deligne, N. I., Guerrero, N. O., et al. (2012). Global database on large magnitude explosive volcanic eruptions (LaMEVE). *Journal of Applied Volcanology*, 1(1), 4. <https://doi.org/10.1186/2191-5040-1-4>
- Degruyter, W., & Bonadonna, C. (2012). Improving on mass flow rate estimates of volcanic eruptions. *Geophysical Research Letters*, 39(16), L16308. <https://doi.org/10.1029/2012GL052566>
- Dioguardi, F., Beckett, F., Dürig, T., & Stevenson, J. A. (2020). The impact of eruption source parameter uncertainties on ash dispersion forecasts during explosive volcanic eruptions. *Journal of Geophysical Research: Atmospheres*, 125(17), e2020JD032717. <https://doi.org/10.1029/2020jd032717>
- Dürig, T., Gudmundsson, M. T., Ágústadóttir, T., Högnadóttir, T., & Schmidt, L. S. (2022). The effect of wind and plume height reconstruction methods on the accuracy of simple plume models - A second look at the 2010 Eyjafjallajökull eruption. *Bulletin of Volcanology*, 84(3), 33. <https://doi.org/10.1007/s00445-022-01541-z>
- Dürig, T., Gudmundsson, M. T., Dioguardi, F., & Schmidt, L. S. (2023). Quantifying the effect of wind on volcanic plumes: Implications for plume modelling. *Journal of Geophysical Research: Atmospheres*, 128(2), e2022JD037781. <https://doi.org/10.1029/2022JD037781>
- Dürig, T., Gudmundsson, M. T., Dioguardi, F., Woodhouse, M., Björnsson, H., Barsotti, S., et al. (2018). REFIR-A multi-parameter system for near real-time estimates of plume-height and mass eruption rate during explosive eruptions. *Journal of Volcanology and Geothermal Research*, 360, 61–83. <https://doi.org/10.1016/j.jvolgeores.2018.07.003>
- Eychenne, J., Le Pennec, J. L., Troncoso, L., Gouhier, M., & Nedelec, J. M. (2012). Causes and consequences of bimodal grain-size distribution of tephra fall deposited during the August 2006 Tungurahua eruption (Ecuador). *Bulletin of Volcanology*, 74(1), 187–205. <https://doi.org/10.1007/s00445-011-0517-5>
- Freret-Lorgeril, V., Bonadonna, C., Corradini, S., Donnadieu, F., Guerrieri, L., Lacanna, G., et al. (2021). Examples of multi-sensor determination of eruptive source parameters of explosive events at Mount Etna. *Remote Sensing*, 13(11), 2097. <https://doi.org/10.3390/rs13112097>
- Freret-Lorgeril, V., Donnadieu, F., Scollo, S., Provost, A., Fréville, P., Guéhenneux, Y., et al. (2018). Mass eruption rates of tephra plumes during the 2011–2015 lava fountain paroxysms at Mt. Etna from Doppler radar retrievals. *Frontiers in Earth Science*, 6, 73. <https://doi.org/10.3389/feart.2018.00073>
- Glaze, L. S., Baloga, S. M., & Wilson, L. (1997). Transport of atmospheric water vapor by volcanic eruption columns. *Journal of Geophysical Research*, 102(D5), 6099–6108. <https://doi.org/10.1029/96JD03125>
- Gouhier, M., Eychenne, J., Azzaoui, N., Guillin, A., Deslandes, M., Poret, M., et al. (2019). Low efficiency of large volcanic eruptions in transporting very fine ash into the atmosphere. *Scientific Reports*, 9(1), 1–12. <https://doi.org/10.1038/s41598-019-38595-7>
- Herzog, M., Graf, H.-F., Textor, C., & Oberhuber, J. M. (1998). The effect of phase changes of water on the development of volcanic plumes. *Journal of Volcanology and Geothermal Research*, 87(1–4), 55–74. [https://doi.org/10.1016/S0377-0273\(98\)00100-0](https://doi.org/10.1016/S0377-0273(98)00100-0)
- Hewett, T. A., Fay, J. A., & Hoult, D. P. (1971). Laboratory experiments of smokestack plumes in a stable atmosphere. *Atmospheric Environment* (1967), 5(9), 767–789. [https://doi.org/10.1016/0004-6981\(71\)90028-x](https://doi.org/10.1016/0004-6981(71)90028-x)
- Kratzmann, D. J., Carey, S. N., Fero, J., Scasso, R. A., & Naranjo, J.-A. (2010). Simulations of tephra dispersal from the 1991 explosive eruptions of Hudson volcano, Chile. *Journal of Volcanology and Geothermal Research*, 190(3), 337–352. <https://doi.org/10.1016/j.jvolgeores.2009.11.021>
- Maeno, F., Nagai, M., Nakada, S., Burden, R., Engwell, S., Suzuki, Y., & Kaneko, T. (2014). Constraining tephra dispersion and deposition from three subplinian explosions in 2011 at Shinmoedake volcano, Kyushu, Japan. *Bulletin of Volcanology*, 76(6), 823. <https://doi.org/10.1007/s00445-014-0823-9>
- Maeno, F., Nakada, S., Yoshimoto, M., Shimano, T., Hokanishi, N., Zaennudin, A., & Iguchi, M. (2019). A sequence of a Plinian eruption preceded by dome destruction at Kelud volcano, Indonesia, on February 13, 2014, revealed from tephra fallout and pyroclastic density current deposits. *Journal of Volcanology and Geothermal Research*, 382, 24–41. <https://doi.org/10.1016/j.jvolgeores.2017.03.002>
- Mastin, L. G., Pavlonis, M., Engwell, S., Clarkson, R., Witham, C., Brock, G., et al. (2022). Progress in protecting air travel from volcanic ash clouds. *Bulletin of Volcanology*, 84(1), 9. <https://doi.org/10.1007/s00445-021-01511-x>
- Mastin, L. G. (2014). Testing the accuracy of a 1-D volcanic plume model in estimating mass eruption rate. *Journal of Geophysical Research: Atmospheres*, 119(5), 2474–2495. <https://doi.org/10.1002/2013jd020604>
- Mastin, L. G., Guffanti, M., Servranckx, R., Webley, P., Barsotti, S., Dean, K., et al. (2009). A multidisciplinary effort to assign realistic source parameters to models of volcanic ash-cloud transport and dispersion during eruptions. *Journal of Volcanology and Geothermal Research*, 186(1–2), 10–21. <https://doi.org/10.1016/j.jvolgeores.2009.01.008>
- Mereu, L., Scollo, S., Bonadonna, C., Donnadieu, F., Freret-Lorgeril, V., & Marzano, F. S. (2022). Ground-based remote sensing and uncertainty analysis of the mass eruption rate associated with the 3–5 December 2015 paroxysms of Mt. Etna. *IEEE Journal of Selected Topics in Applied Earth Observations and Remote Sensing*, 15, 504–518. <https://doi.org/10.1109/JSTARS.2021.3133946>
- Mereu, L., Scollo, S., Garcia, A., Sandri, L., Bonadonna, C., & Marzano, F. S. (2023). A new radar-based statistical model to quantify mass eruption rate of volcanic plumes. *Geophysical Research Letters*, 50(7), e2022GL100596. <https://doi.org/10.1029/2022gl100596>
- Michaud-Dubuy, A., Carazzo, G., & Kaminski, E. (2020). Wind entrainment in jets with reversing buoyancy: Implications for volcanic plumes. *Journal of Geophysical Research: Solid Earth*, 125(10), e2020JB020136. <https://doi.org/10.1029/2020JB020136>
- Morton, B. R., Taylor, G. I., & Turner, J. S. (1956). Turbulent gravitational convection from maintained and instantaneous sources. *Proceedings of the Royal Society of London. Series A. Mathematical and Physical Sciences*, 234(1196), 1–23.
- Naranjo, J., Sigurdsson, H., Carey, S., & Fritz, W. (1986). Eruption of the Nevada del Ruiz volcano, Colombia, on 13 November 1985: Tephra fall and lahars. *Science*, 233(4767), 961–964. <https://doi.org/10.1126/science.233.4767.961>
- Newhall, C. G., & Self, S. (1982). The volcanic explosivity index (VEI) an estimate of explosive magnitude for historical volcanism. *Journal of Geophysical Research*, 87(C2), 1231–1238. <https://doi.org/10.1029/jc087ic02p1231>
- Pioli, L., & Harris, A. J. (2019). Real-time geophysical monitoring of particle size distribution during volcanic explosions at Stromboli volcano (Italy). *Frontiers in Earth Science*, 7, 52. <https://doi.org/10.3389/feart.2019.00052>
- Poullidis, A. P., Takemi, T., & Iguchi, M. (2019). The effect of wind and atmospheric stability on the morphology of volcanic plumes from vulcanian eruptions. *Journal of Geophysical Research: Solid Earth*, 124(8), 8013–8029. <https://doi.org/10.1029/2018JB016958>
- Romero, J. E., Vera, F., Polacci, M., Morgavi, D., Arzilli, F., Alam, M. A., et al. (2018). Tephra from the 3 March 2015 sustained column related to explosive lava fountain activity at Volcán Villarrica (Chile). *Frontiers in Earth Science*, 6, 98. <https://doi.org/10.3389/feart.2018.00098>
- Rosi, M., Paladio-Melosantos, M., Di Muro, A., Leoni, R., & Bocolcol, T. (2001). Fall vs flow activity during the 1991 climactic eruption of Pinatubo Volcano (Philippines). *Bulletin of Volcanology*, 62(8), 549–566. <https://doi.org/10.1007/s004450000118>

- Rossi, E., Bonadonna, C., & Degruyter, W. (2019). A new strategy for the estimation of plume height from clast dispersal in various atmospheric and eruptive conditions. *Earth and Planetary Science Letters*, 505, 1–12. <https://doi.org/10.1016/j.epsl.2018.10.007>
- Scollo, S., Prestifilippo, M., Bonadonna, C., Cioni, R., Corradini, S., Degruyter, W., et al. (2019). Near-real-time tephra fallout assessment at Mt. Etna, Italy. *Remote Sensing*, 11(24), 2987. <https://doi.org/10.3390/rs11242987>
- Self, S., & Rampino, M. (2012). The 1963-1964 eruption of Agung volcano (Bali, Indonesia). *Bulletin of Volcanology*, 74(6), 1521–1536. <https://doi.org/10.1007/s00445-012-0615-z>
- Sparks, R. S. J. (1986). The dimensions and dynamics of volcanic eruption columns. *Bulletin of Volcanology*, 48(1), 3–15. <https://doi.org/10.1007/bf01073509>
- Spieß, A. N., & Neumeier, N. (2010). An evaluation of R^2 as an inadequate measure for nonlinear models in pharmacological and biochemical research: A Monte Carlo approach. *BMC Pharmacology*, 10(1), 6. <https://doi.org/10.1186/1471-2210-10-6>
- Trancoso, R., Behr, Y., Hurst, T., & Deligne, N. I. (2022). Towards real-time probabilistic ash deposition forecasting for New Zealand. *Journal of Applied Volcanology*, 11(1), 13. <https://doi.org/10.1186/s13617-022-00123-0>
- Tupper, A., Textor, C., Herzog, M., Graf, H.-F., & Richards, M. S. (2009). Tall clouds from small eruptions: The sensitivity of eruption height and fine ash content to tropospheric instability. *Natural Hazards*, 51(2), 375–401. <https://doi.org/10.1007/s11069-009-9433-9>
- Tupper, A., & Wunderman, R. (2009). Reducing discrepancies in ground and satellite-observed eruption heights. *Journal of Volcanology and Geothermal Research*, 186(1–2), 22–31. <https://doi.org/10.1016/j.jvolgeores.2009.02.015>
- Wilson, L., Sparks, R. S. J., Huang, T. C., & Watkins, N. D. (1978). The control of volcanic column heights by eruption energetics and dynamics. *Journal of Geophysical Research*, 83(B4), 1829–1836. <https://doi.org/10.1029/jb083ib04p01829>
- Wilson, L., & Walker, G. P. L. (1987). Explosive volcanic eruptions-VI. Ejecta dispersal in Plinian eruptions: The control of eruption conditions and atmospheric properties. *Geophysical Journal International*, 89(2), 657–679. <https://doi.org/10.1111/j.1365-246x.1987.tb05186.x>
- Woodhouse, M. J., Hogg, A. J., Phillips, J. C., & Sparks, R. S. J. (2013). Interaction between volcanic plumes and wind during the 2010 Eyjafjallajökull eruption, Iceland. *Journal of Geophysical Research: Solid Earth*, 118(1), 92–109. <https://doi.org/10.1029/2012jb009592>
- Woods, A. W. (1988). The fluid dynamics and thermodynamics of eruption columns. *Bulletin of Volcanology*, 50(3), 169–193. <https://doi.org/10.1007/BF01079681>
- Woods, A. W. (1993). Moist convection and the injection of volcanic ash into the atmosphere. *Journal of Geophysical Research*, 98(B10), 17627–17636. <https://doi.org/10.1029/93JB00718>

References From the Supporting Information

- Bonadonna, C., Biass, S., & Costa, A. (2015c). Physical characterization of explosive volcanic eruptions based on tephra deposits: Propagation of uncertainties and sensitivity analysis. *Journal of Volcanology and Geothermal Research*, 296, 80–100. <https://doi.org/10.1016/j.jvolgeores.2015.03.009>